Influence of Deposition and Annealing Temperature on Resistivity and Nanoindentation Characteristics of Reactive Magnetic Sputtered NiO Films

Kumar, Mukesh*+

Department of Physics, Faculty of Science, Shree Guru Gobind Singh Tricentenary University Gurgaon-122001, Delhi-NCR, INDIA

Ansari, Jamilur R.

Department of Applied Science & Humanities, Dronacharya College of Engineering, Khentawas, Farrukh Nagar, Gurugram-123506, Haryana, INDIA

Srivastava, Ashok Kumar

Amity University, Jharkhand, Ranchi-834002, INDIA

Sharma, Ashutosh*+

Department of Materials Science and Engineering, 206-Worldcup-ro, Yeongtong-gu, Suwon 16499, Gyeonggi-do, Republic of KOREA

ABSTRACT: *In this study, NiO films were processed on p-type Si by magnetron sputtering technique under the mixture of argon (Ar) and oxygen (O_2) gas atmosphere at room temperature and 300 ^{0}C. The microstructure, nanoindentation, and electrical properties of the NiO films were compared with the as-deposited and subsequent vacuum-annealed films at 300 ^{0}C for one hour. The grain size and phase structure of NiO films were determined by an X-ray diffraction study. The microstructure and morphology of the resultant NiO films were analyzed by Field Emission Scanning Electron Microscopy (FESEM) and transmission electron microscopy (TEM). The results show that NiO films were nanocrystalline with grain size in the range of 14-32 nm. The formation of $NiSi_2$ was noticed at the interface of vacuum-annealed NiO films. Nanoindentation results showed an increment in the hardness of annealed NiO films over as-deposited films at the same temperature. In contrast, Van der Pauw's four-point probe method showed a reduced resistivity of vacuum-annealed NiO films which can be potential candidates for electrical contact applications.*

KEYWORDS: *NiO films; Magnetron sputtering; Vacuum annealing; Microstructure; Electrical properties.*

INTRODUCTION

Nanocrystalline NiO films have gained worldwide attention because of their great applications in the field of sensors, the automobile industry, solar cells, supercapacitors, and spintronics because of their fantastic

* *To whom correspondence should be addressed.*

+ E-mail: mukesh.kumar@sgtuniversity.org , a4ashu2003@gmail.com

1021-9986/2023/10/3249-3256 13/$/6.03

Table 1: Parameters for the magnetron sputtering of NiO films during processing

Process parameters	Values
Base pressure	2.0×10^{-6} Torr
Working pressure	30 m Torr
Ar:O_2	1:1
Ni DC power	100 W
Ar and O_2 flow rate	50 sccm
Substrate temperature	26 °C and 300 °C
Vacuum annealing	300 °C
Substrate-Target distance	150 mm
Substrate rotation	25 rpm
Duration for deposition	1 hour

optical, magnetic, and electrical properties along with excellent chemical durability [1–7]. Furthermore, NiO films have a p-type direct band gap semiconductor that is in the 3.6–4.0 eV range [8], making them appropriate for use in metal–oxide–semiconductor (MOS) devices. Additionally, nickel silicides ($NiSi_2$, Ni_2Si, NiSi, etc.), which are anticipated to form during the annealing of NiO films, have been extensively used in optoelectronic and contemporary microelectronic devices due to their low resistance and midgap work function, making them more suitable for contact applications in electronic devices [1,6,9,10].

Scientists across the globe have reported that metal oxide films were mostly studied in the fields of semiconductor devices, bio/chemical sensors, photocatalytic activities, etc. applications as these possess excellent physical and chemical properties [26–29]. *Hotový et al* [30] in their study have discussed that the electrical properties of sputtered NiO films increase efficiently with the increase in oxygen content of NiO films [31]. It has also been observed that increasing the annealing temperature of spin-coated NiO films causes a considerable decrease in electrical resistivity [31-33]. The gas-sensing properties of NiO films were also verified by *Liyo* and *Abirami* [34,35]. Recently, *Zhao et al* [10] studied the influence of the partial pressure of oxygen on the optical and electrical resistivity of NiO films.

Previous studies have described the creation of NiO films by a number of physical and chemical vapor deposition techniques, such as thermal evaporation, electrochemical deposition, spray pyrolysis, magnetron sputtering, and chemical solution deposition [11–16]. The processing of the examined films was found to benefit from magnetron sputtering the most out of these approaches. This technique provides better control of the purity of the processed films [17–22]. This technique also monitors the surface morphology and grain size distribution in the investigated films by regulating the parameters in particular substrate temperature, substrate bias, target power etc. [2,23–25]. The physical and chemical characteristics of the NiO films can be controlled by the process parameters linked to magnetron sputtering, specifically, substrate temperature, vacuum annealing, partial pressure of oxygen, etc [26,36-38]. Therefore, in this study, authors have analyzed the impact of vacuum annealing and substrate temperature on the microstructure and electrical characteristics of magnetic sputtered NiO films.

EXPERIMENTAL SECTION

NiO thin film processing

NiO films were grown on p-type Si <100> substrates using a Direct Current (DC) magnetron sputtering machine (KVST-4065 model, Korea Vac. Technology) with Ni target under a pure Ar and O_2 inert atmosphere. Around 2×10^{-6} Torr base pressure was attained for the deposition using a rotary and turbomolecular combination. The flow rate Ar/O_2 gas was maintained at 50 sccm by a throttle valve, while the pressure inside the chamber was measured by MKS Baraton gauge. The NiO films were sputtered at room temperature (RT, 26 ^{0}C) and 300 ^{0}C respectively. Further, as-deposited films were vacuum annealed at 300 ^{0}C using a heating element of SiC attached to the substrate holder. The various processing constraints used for the sputtering experiment are presented in Table 1.

Table 2: Microstrain and grain size of the processed NiO films

Temperature (^{0}C)	Strain ($\times 10^{-3}$)	Grain size (nm)
Deposition at RT	3.9 ± 0.4	14.2 ± 0.5
Deposition at 300	2.3 ± 0.5	32.5 ± 0.5
Vacuum annealed at 300	1.9 ± 0.4	30.4 ± 0.4

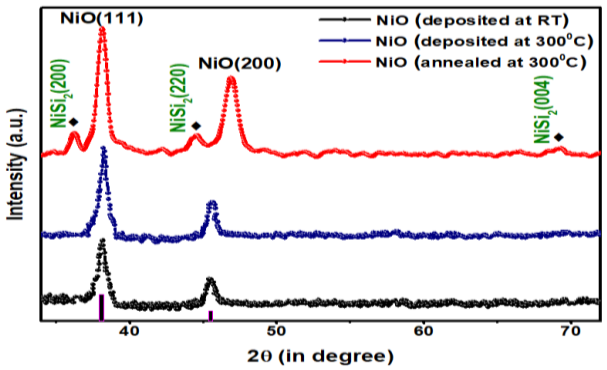

Fig. 1: GIXRD patterns of NiO films processed at various conditions

Characterization

The surface profilometer was used to measure the NiO films' thickness (Dektak 150, USA). To analyze the current phases and crystallinity of the produced films, the grazing incidence mode of X-ray diffraction (GIXRD, Philips X'Pert PRO) was taken into consideration. Utilizing Cu K radiation with a wavelength of 1.54, GIXRD was activated at operating parameters of 40 kV and 30 mA with a scanning rate of 0.05/s. A FESEM (Zeiss Supra, Germany) coupled with an Energy-Dispersive X-ray spectrometer (EDX) was employed to perform the morphology and compositional analyses. TEM (JEOL-JEM 2100, Japan) was also used for detailed microstructural examination. TEM samples were prepared by mechanical thinning (Model 656 Gatan Inc.) followed by milling using Ar+ (model 691, Gatan Inc.).

The nanoindentation properties of the samples were determined by a nanoindenter (Berkovich tip; UNATS, ASMEC Nanomechanical tester, Germany). The tests were done at 30 locations up to 2000 µN and the load-depth profiles were recorded.

The electrical resistivity of the films was analysed using the Van-der Pauw four-point probe method at ohmic contacts with a 2 mm separation (Keithley 220 current source and 2182 nano-voltmeter, USA) [39]. Additionally, a constant current of 1 mA was recorded as the voltage drop across the inner probe. The resistivity (ρ) of the samples was derived from equation (1) using the calculated resistance R.

$$\rho = \frac{RA}{s} = \frac{V}{I}\frac{d \times t}{s} \quad (1)$$

Where ρ is the resistivity, t is the thickness of the deposited film, d is the substrate width and s is the probe spacing. I and V are the applied current and voltages.

RESULTS AND DISCUSSION

XRD analysis

The characteristic XRD peaks of the processed NiO films at various process conditions are shown in Fig. 1. Fig. 1 depicts the presence of NiO phase with face-centered cubic structure (FCC) which matches the standard XRD database of ICDD (PDF # 47-1049) with ideal orientation in <111> direction. There was no big difference in phase evolution of as-deposited NiO films at RT and 300ºC, except for the smaller crystallite size (~14 nm) of RT-deposited films than those deposited at 300ºC (~32 nm). While nickel silicide ($NiSi_2$) phase along with the NiO phase is observed with diamond marks with (200), (220), and (004) planes in annealed films.

The observed peaks (200), (220), and (004) are indexed with FCC structure and are consistent with their analogous bulk counterpart which further confirms the formation of $NiSi_2$ phase [40–42]. The developed microstrain and the average grain sizes were measured with the help of Williamson-Hall relation [43] as given in Table 2.

We observed that there is a drop in the value of microstrain with increasing substrate temperature which occurred due to uniform deposition of NiO films at relatively high temperatures. Due to the increase in adatoms mobility, there was a decrease in the rate of nucleation site formation which occurred at higher temperatures, which leads to the formation of coarser grain size in NiO films.

Microstructural and elemental analysis

The plane view FESEM images of the sputtered NiO films at RT, 300℃ and annealed at 300 ^{0}C for 1 h are shown in Fig. 2a-d, respectively. It can be seen that the size of the NiO films deposited at RT had fine grains which increased with deposition at higher temperatures (300ºC) (Fig. 2a, b). Further, there were slight differences in the microstructure of NiO films after post-annealing at 300 ^{0}C.

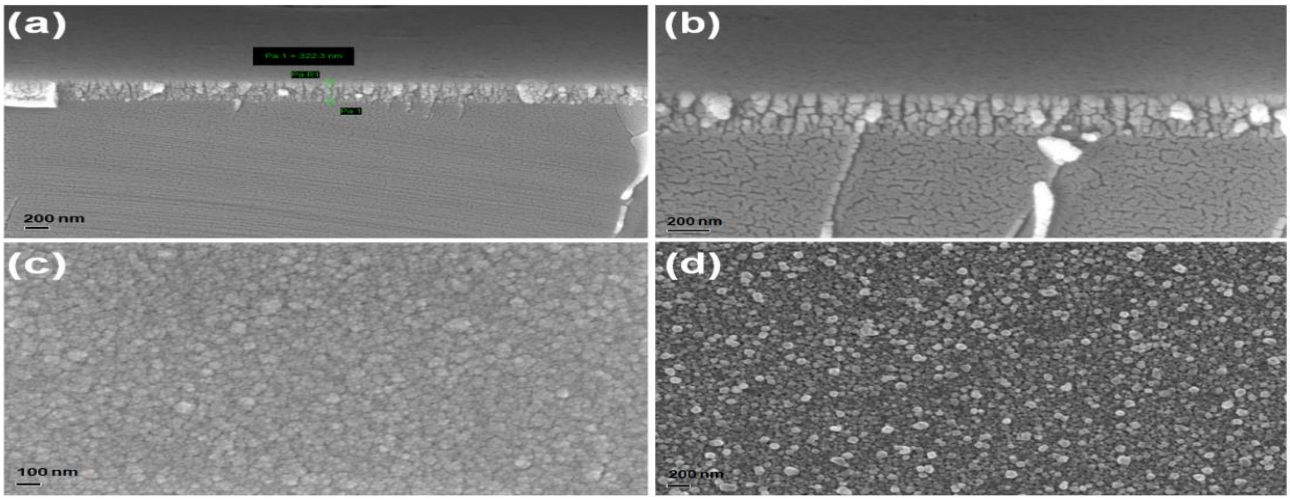

Fig. 2: FESEM images of the nanocrystalline NiO films deposited at (a) RT (26 ^{0}C), (b) 300 ^{0}C, and (c, d) vacuum annealed at 300 ^{0}C

The cross-sectional FE-SEM morphologies of the NiO films annealed at 300 ^{0}C as shown in Fig. 2c-d shows the coalescence of individual islands which leads to columnar microstructure. During lower temperature deposition of NiO films, limited atomic mobility on the substrate confine nucleation sites on the substrate which ultimately leads to the growth of film vertically instead of laterally. An ideal condition for the deposition is that the growth rate should be equal to the nucleation rate to lead to smooth-continuous films with higher density. Nevertheless, this study reveals that the adatoms deposition rate is smaller than the rate of nuclei formation. Thus, there is individual growth of the island microstructure.

TEM imaging

To investigate the phase evolution at the NiO/Si interface, cross-sectional TEM analysis was done for NiO films vacuum annealed at 300^{o}C. The results are shown in Fig. 3a-d. The cross-sectional bright and dark field TEM images of NiO film annealed at 300°C are shown in Fig.3a-b, respectively. These images clearly show the formation of nickel silicides ($NiSi_2$) at the interface. Selected Area Electron Diffraction (SAED) patterns consisting of circular rings are indexed to NiO phase as well as $NiSi_2$ phase as shown in Fig.3c-d. The formation of $NiSi_2$ was also detected in XRD analysis (Fig. 1) for NiO films vacuum annealed at 300 ^{0}C temperature. Furthermore, close observation of cross-sectional TEM images shows the existence of a homogeneous thin region grown between the Si interface and NiO film (represented by blue arrows) because of interfacial diffusion. The interfacial diffused region at the interface between NiO/Si substrate is expected to provide a path for the inter-diffusion of Ni and Si atoms across NiO/Si interface. A similar formation of nickel silicides has been reported by *Qiu et al* [44] in the case of Ni films reactively sputtered on Si substrate at 200 ^{0}C.

The high-resolution TEM image reveals the lattice planes of NiO (111) and $NiSi_2$ (200) films as shown in Fig. 3c. Fig. 3d represents the SAED pattern taken at the interfacial area of NiO film–Si substrate. The observed some of the un-indexed spots of the diffraction pattern are the indication of the presence of other phases NiO, and Si apart from $NiSi_2$ at the interface.

Nanohardness

The load-depth nanoindentation graphs depicting the nanohardness (H_T) values of the investigated NiO films are presented in Fig. 4a. Fig. 4b shows the corresponding surface topography of NiO films annealed at 300 ^{o}C. The measured values of nanohardness of the different samples are shown in Fig. 4c. These results show that the deposition temperature and annealing temperatures affect the nanohardness of the sputtered NiO films. The nanohardness values of NiO films estimated in the present investigation are in the range of 3.5–8.2 GPa with the highest hardness for the annealed NiO films. Sputter-deposited Ni films are reported with hardness values of 3.12 GPa, while the hardness value of bulk Ni is 2.45 GPa [31]. Higher hardness values for the NiO films deposited at 300 ^{o}C and vacuum annealed at 300 ^{o}C are expected due to

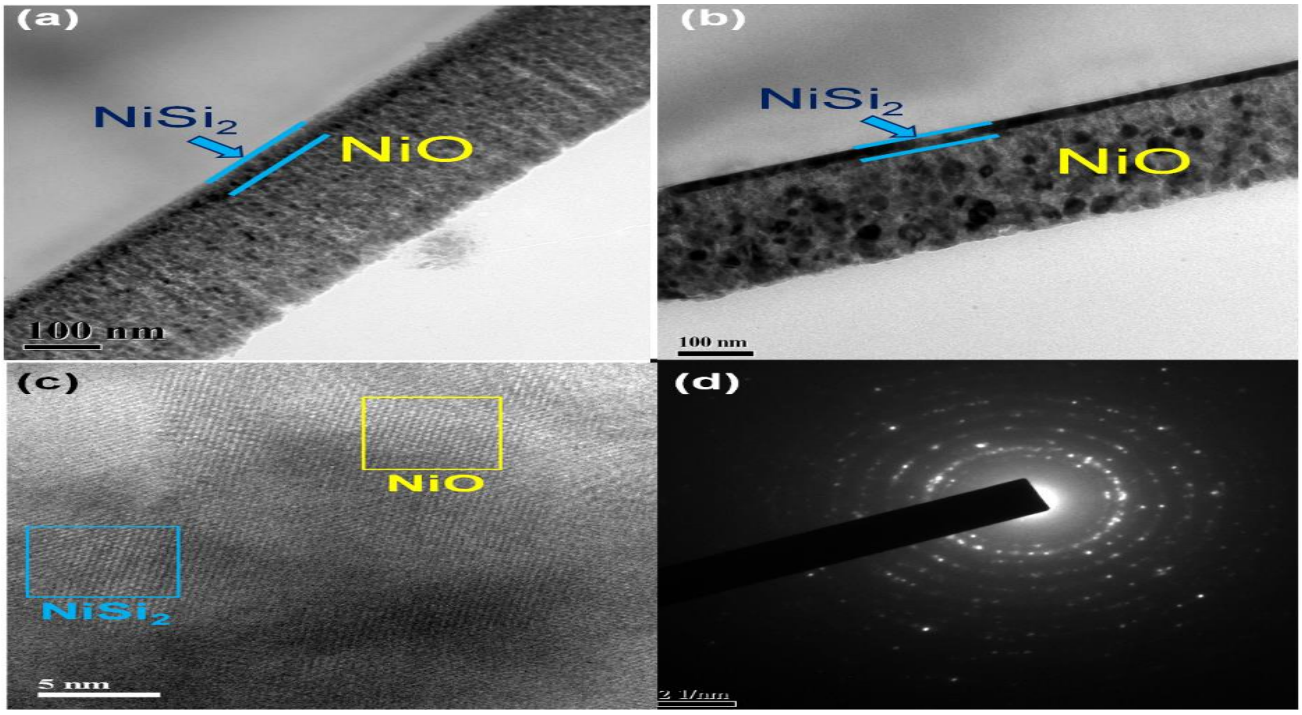

Fig. 3: TEM images of the NiO films annealed at 300°C. (a-b) Bright and dark field image of NiO, (c) High resolution TEM image of NiO/NiSi2, and (c) SAED pattern

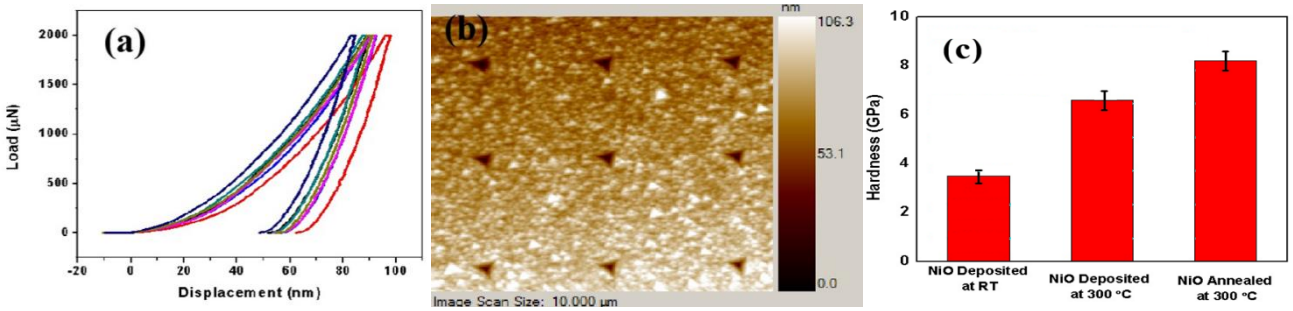

Fig. 4: (a) Load vs displacement plot, (b) corresponding surface topography of indents, and (c) bar chart for the Nanohardness values of various samples

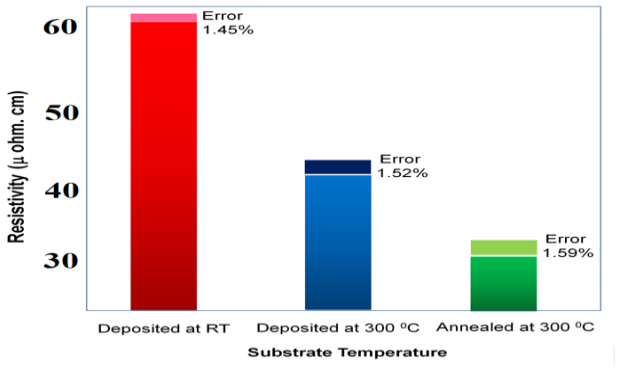

Fig. 5: Electrical resistivity of the NiO films deposited at various conditions

to the formation of $NiSi_2$ phase which has been confirmed by both XRD and TEM results.

Electrical resistivity

The value of resistivity calculated from the I-V characteristic is expressed by Equation 1. Fig. 5 shows the comparison of the electrical resistivity of the NiO films deposited at RT (26 ℃), 300 °C, and vacuum annealed at 300 °C. The results show that the NiO films deposited at 300 ^{0}C as well as vacuum annealed samples at 300 ^{0}C possess lower electrical resistivity as compared to those deposited at RT varying from 36 μΩ.cm to 62 μΩ.cm.

Due to the formation of the $NiSi_2$ at the interface, there was a decrease in the electrical resistivity of the annealed NiO films.

The electrons are get scattered by the presence of phonons as well as impurities inside the processed films. Wherever the current flows in the region comparable to nano-size, the scattering of electrons occurs on the surface which is called surface scattering. Therefore, it is necessary to investigate the existence of the grain inside the NiO films as well as $NiSi_2$ at the interface. It was seen that NiO thin films sputtered at lower temperature exhibits mainly p-type conductivity. However, for the NiO thin films post-annealed at 300°C, the resistivity decreases drastically due to the inclusion of majority carriers in the form of electrons contributed by the metallic $NiSi_2$ which shows the n-type conductivity. Moreover, the higher resistivity for the NiO films processed at RT can be the effect of grain boundary scattering along with the surface scattering. The resistivity values indicate that the $NiSi_2$ phase is metallic. A good agreement with this observation is seen in the previous results [40, 41, 44].

CONCLUSIONS

Reactive magnetron sputtering, which we successfully used to deposit NiO thin films, revealed the existence of nickel silicides at the interface, which was further validated by GIXRD and TEM examination. Additionally, GIXRD reveals the presence of nanocrystalline NiO phases with the predominant orientation being in the (111) plane and grain sizes ranging from 12-32 nm. The cross-section TEM micrographs reveal a more uniform distribution of grains for the films processed at 300 ^{0}C and the formation of $NiSi_2$ phase was evident. The nanoindentation results showed increased hardness in annealed samples due to the formation of harder $NiSi_2$ interfacial compounds as confirmed by the XRD and TEM results. The analysis of electrical resistivity obtained by four probe method show the variation from 62 μΩ.cm to 36 μΩ.cm with the increase in substrate temperature from ambient to 300 ^{0}C as well as in vacuum annealed samples. A smaller electrical resistivity in annealed samples was due to the formation of the metallic $NiSi_2$ phase which decreases the resistivity of NiO films. We also observed that electrical resistivity was correlated with the grain size and it decreases with increasing the grain size.

Acknowledgement

Authors are thankful to Indian Institute of Technology Kharagpur, Shree Guru Gobind Singh Tricentenary University and Dronacharya College of Engineering, Gurgaon, Delhi-NCR for their supports.

Received : Jan. 02, 2023 ; Accepted : Apr.14, 2023

REFERENCES

[1] Decker C.A., Solanki R., Freeouf J.L., Carruthers J.R., Evans D.R., Directed Growth of Nickel Silicide Nanowires, *Appl. Phys. Lett.*, **84**: 1389–1391(2004).

[2] Kumar M., Effect of Substrate Temperature on Surface Morphology and Optical Properties of Sputter Deposited Nanocrystalline Nickel Oxide Films, *Mater. Res. Express*, **6**: 096404 (2019).

[3] Padhan A.M., Ravikumar P., Saravanan P., Alagarsamy P., Enhanced Magnetic Properties of NiO Powders by the Mechanical Activation of Aluminothermic Reduction of NiO Prepared by a Ball Milling Process, J. *Magn. Magn. Mater*, **418**: 253–259 (2016).

[4] Okumura T., Sugiyo T., Inoue T., Ikegami M., Miyasaka T., Nickel Oxide Hybridized Carbon Film as an Efficient Mesoscopic Cathode for Dye-Sensitized Solar Cells, *J. Electrochem. Soc.*, **160**: H155–H159(2013).

[5] Kemary M. El., Nagy N., I. El-Mehasseb, Nickel Oxide Nanoparticles: Synthesis and Spectral Studies of Interactions with Glucose, *Mater. Sci. Semicond. Process.*, **16**: 1747–1752(2013).

[6] Kim J.,. Bae J.-U, Anderson W.A., Kim H.-M., Kim K.-B., Solid-State Growth of Nickel Silicide Nanowire by the Metal-Induced Growth Method, *J. Mater. Res.*, **21**: 2936–2940 (2006).

[7] Salehirad A., Synthesis of High Surface Area NiO Nanoparticles through Thermal Decomposition of Mixed Ligand Ni(II) Complex, [Ni(binol)(bpy)]·CH3OH, *Russ. J. Appl. Chem.*, **89**: 63–69 (2016).

[8] Menaka S.M., Umadevi G., Concentration Dependent Structural, Morphological, Spectral, Optical and Electrical Properties of Spray Pyrolyzed NiO thin Films, *Silicon.*, **10**: 2023–2029 (2018).

[9] Carbone M., NiO-Based Electronic Flexible Devices, *Appl. Sci.*, **12**: 2839 (2022).
[10] Zhao Y., Wang H., Wu C., Z. Shi F., Gao F.B., W Li. C., Wu G.G., Zhang B.L., Du G.T., Structures, Electrical and Optical Properties of Nickel Oxide Films by Radio Frequency Magnetron Sputtering, *Vacuum*, **103**: 14–16 (2014).
[11] I Fasaki., Koutoulaki A., Kompitsas M., Charitidis C., Structural, Electrical and Mechanical Properties of NiO thin Films Grown by Pulsed Laser Deposition, *Appl. Surf. Sci*. **257**: 429–433(2010).
[12] Kang J.-K., Rhee S.-W., Chemical Vapor Deposition of Nickel Oxide Films from $Ni(C_5H_5)_2/O_2$, *Thin Solid Films*, **391**: 57–61(2001).
[13] Desai J.D., Min S.-K., Jung K.-D., Joo O.-S., Spray Pyrolytic Synthesis of Large Area NiOx thin Films from Aqueous Nickel Acetate Solutions, *Appl. Surf. Sci.*, **253**: 1781–1786(2006).
[14] Nakaoka K., Ueyama J., Ogura K., Semiconductor and Electrochromic Properties of Electrochemically Deposited Nickel Oxide Films, *J. Electroanal. Chem*., **571**: 93–99 (2004).
[15]Garcia-Miquel J.L., Zhang Q., Allen S.J., A Rougier., Blyr A., Davies H.O., Jones A.C., Leedham T.J., P Williams.A., Impey S.A., Nickel Oxide Sol–Gel Films from Nickel Diacetate for Electrochromic Applications, *Thin Solid Films*., **424**: 165–170(2003).
[16] Taylor D.J., P Fleig. F., S Schwab. T., Page R.A., Sol–Gel Derived, Nanostructured Oxide Lubricant Coatings, *Surf. Coat. Technol*. 120–121 465–469(1999).
[17] Park J.-W., Park J.-W., Kim D.-Y.,. Lee J.-K, Reproducible Resistive Switching in Nonstoichiometric Nickel Oxide Films Grown by Rf Reactive Sputtering for Resistive Random-Access Memory Applications, *J. Vac. Sci. Technol. Vac. Surf. Films*., **23**: 1309–1313(2005).
[18]Ahn K.-S., Y Nah.-C., Sung Y.-E., Surface Morphological, Microstructural, and Electrochromic Properties of Short-Range Ordered and Crystalline Nickel Oxide Thin Films, *Appl. Surf. Sci*. **199:** 259–269 (2002).
[19] Chen H.-L., Lu Y.-M., Hwang W.-S., Thickness Dependence of Electrical and Optical Properties of Sputtered Nickel Oxide Films, *Thin Solid Films*., **514**: 361–365(2006).
[20] Pramanik P., Bhattacharya S., A Chemical Method for the Deposition of Nickel Oxide Thin Films, *J. Electrochem. Soc*., **137**: 3869–3870 (1990).
[21] Pejova B., Kocareva T., M Najdoski., Grozdanov I., A Solution Growth Route to Nanocrystalline Nickel Oxide Thin Films, *Appl. Surf. Sci.*, **165**: 271–278(2000).
[22] Varkey A.J., Fort A.F., Solution Growth Technique for Deposition of Nickel Oxide thin Films, *Thin Solid Films.*, **235**: 47–50 (1993).
[23] Kumar M., Sharma A., Microstructure, Mechanical, and Nanotribological Properties of Ni, Ni-TiN, and Ni90Cu10-TiN Films Processed by Reactive Magnetron Cosputtering, *Adv. Mater. Sci. Eng*., **2022:** 9391183(2022).
[24] Kumar M., Mitra R., Effect of Substrate Temperature and Annealing on Structure, Stress and Properties of Reactively Co-Sputtered Ni-TiN Nanocomposite thin Films, *Thin Solid Films.*, **624**: 70–82(2017).
[25] Kumar M., Shetti N.P., Magnetron Sputter Deposited NiCu Alloy Catalysts for Production of Hydrogen through Electrolysis in Alkaline Water, *Mater. Sci. Energy Technol*., **1**: 160–165 (2018).
[26] Brioual B., Rossi Z., Aouni A., Diani M., Addou M., Jbilou M., Electrochemical Behavior of Spray Deposited Nickel Oxide (NiO) thin Film in Alkaline Electrolyte, *E3S Web Conf.*, **336**: 00045(2022).
[27] Mandal R., Baranwal A., Srivastava A., Chandra P., Evolving Trends in Bio/Chemical Sensor Fabrication Incorporating Bimetallic Nanoparticles, *Biosens. Bioelectron.*, **117**: 546–561(2018).
[28] Saxena V., Chandra P., Pandey L.M., Design and Characterization of Novel Al-Doped ZnO Nanoassembly as an Effective Nanoantibiotic, *Appl. Nanosci*., **8**: 1925–1941(2018).
[29] Kadian S., Arya B.D., Kumar S., S Sharma.N., Chauhan R.P., Srivastava A., Chandra P., Singh S.P., Synthesis and Application of PHT-TiO_2 Nanohybrid for Amperometric Glucose Detection in Human Saliva Sample, *Electroanalysis*, **30**: 2793–2802(2018).
[30] Hotový I., Búc D., Haščík Š., Nennewitz O., Characterization of NiO thin Films Deposited by Reactive Sputtering, *Vacuum*., **50**: 41–44(1998).

[31] Barshilia H.C., K. Rajam S., Characterization of Cu/Ni Multilayer Coatings by Nanoindentation and Atomic Force Microscopy, *Surf. Coat. Technol*., **155**: 195–202(2002).

[32] Kim S.-K., Seok H.-J., Kim D.-H., Choi D.-H., Nam S.-J., Kim S.-C., Kim H.-K., Comparison of NiOx thin Film Deposited by Spin-Coating or Thermal Evaporation for Application as a Hole Transport Layer of Perovskite Solar Cells, *RSC Adv.*, **10**: 43847–43852 (2020).

[33] Napari M., Huq T.N., Hoye R.L.Z., MacManus-Driscoll J.L., Nickel Oxide thin Films Grown by Chemical Deposition Techniques: Potential and Challenges in Next-Generation Rigid and Flexible Device Applications, *InfoMat*. **3(5)**: 536–576(2021).

[34] C Luyo., Ionescu R., Reyes L.F., Topalian Z., W Estrada., Llobet E., Granqvist C.G., Heszler P., Gas Sensing Response of NiO Nanoparticle Films Made by Reactive Gas Deposition, *Sens. Actuators B Chem.*, **138**: 14–20(2009).

[35] Abirami A., Wilson K.S., Structural and Optical Properties on Nickel Oxide thin Films Prepared by Simple Nebulizer Spray Technique, *In: Jodhpur, India*, **2265 (1)**: 030561 (2020).

[36] Salunkhe P., A V M.A., Kekuda D., Investigation on Tailoring Physical Properties of Nickel Oxide thin Films Grown by dc Magnetron Sputtering, *Mater. Res. Express*., **7(1)**: 016427(2020).

[37] Jamal M.S., Chowdhury M.S., Bajgai S., Hossain M., Laref A., Jha P.K., Techato K., Comparative Studies on the Morphological, Structural and Optical Properties of NiO thin Films Grown by Vacuum and Non-Vacuum Deposition Techniques, *Mater. Res. Express*., **8**: 126404(2021).

[38] Ivanova T., Harizanova A., Shipochka M., Vitanov P., Nickel Oxide Films Deposited by Sol-Gel Method: Effect of Annealing Temperature on Structural, Optical, and Electrical Properties, *Materials.*, **15**: 1742 (2022).

[39] Oliveira F.S., Cipriano R.B., da Silva F.T., E Romão.C., dos Santos C.A.M., Simple Analytical Method for Determining Electrical Resistivity and Sheet Resistance Using the Van Der Pauw Procedure, *Sci. Rep*. **10**: 16379(2020).

[40] Lin Y.-R., Tsai W.-T., Wu Y.-C., Lin Y.-H., Ultra Thin Poly-Si Nanosheet Junctionless Field-Effect Transistor with Nickel Silicide Contact, *Materials.*, **10**: 1276: (2017).

[41] Utlu G., Artunç N., Budak S., Tari S., Structural and Electrical Characterization of the Nickel Silicide Films Formed at 850°C by Rapid Thermal Annealing of the Ni/Si(100) Films, *Appl. Surf. Sci*. **256**: 5069–5075 (2010).

[42] Li Y., Gao Y., Yao Y., Sun S., Khatiwada D., Pouladi S., Galstyan E., Rathi M., Dutta P., Litvinchuk A.P., Ryou J.-H., Selvamanickam V., Direct Synthesis of Biaxially Textured Nickel Disilicide Thin Films by Magnetron Sputter Deposition on Low-Cost Metal Tapes for Flexible Silicon Devices, *Appl. Phys. Lett*., **114**: 083502(2019).

[43] Jabir S.A.-A., Harbbi K.H., A Comparative Study of Williamson-Hall Method and Size-Strain Method through X-Ray Diffraction Pattern of Cadmium Oxide Nanoparticle, *In AIP Conference Proceedings*, **2307(1)**: 020015 (2020).

[44] Qiu H., Tian Y., Hashimoto M., Evolution of Interface Diffusion and Structure of Ni Films Sputter-Deposited on Si(001), *Vacuum*, **70**: 493–497(2003).